29th Congress of the International Council of the Aeronautical Sciences
St. Petersburg, Russia; September 7–12, 2014

A RAPID ANALYSIS METHODOLOGY FOR EARTH ENTRY VEHICLE DEVELOPMENT

Scott Perino*, Javid Bayandor*
***Crashworthiness for Aerospace Structures and Hybrids (CRASH) Lab**
Dept. of Mechanical Engineering, Virginia Tech, Blacksburg, VA, 24061

Keywords: *reentry vehicle, structural dynamics, Mars sample return, multi-mission, EEV*

Abstract

Development of an Earth Entry Vehicle and the methodology created to evaluate its structural dynamic response during launch is reported. NASA's future Mars Sample Return Mission requires a robust vehicle to return Martian samples back to Earth for examination. The Earth Entry Vehicle is NASA's solution to this Mars Sample Mission requirement. During launch the vehicle may experience large structural loads. To decrease development time and cost, a parametric and automated finite element analysis methodology has been developed. Models are built using a software coding technique, which allows modification to all aspects of the model including: geometry, material properties, load and boundary conditions, mesh grids, and analysis controls. The methodology allows data to be rapidly generated for a vast array of potential vehicle configurations. Analyses including quasi-static inertial, structure-borne vibration frequency response, and random acoustic analyses are conducted for the parametric analysis. To demonstrate the parametric analysis capability of the methodology, mesh density and cone angle parameters were varied and then all analyses were executed. The analysis methodology is shown to facilitate and expedite future cost-effective planetary exploration missions.

1 Introduction

Throughout space exploration history, humans have been collecting and testing extraterrestrial materials. Numerous lunar samples have been collected since the Apollo missions and now there is a desire to learn more about our universe by collecting samples from Mars and other planets. To date, the information obtained about Mars has been acquired through the use of rovers such as the recently deployed NASA Curiosity rover, deep space telescopes, and spacecraft with specialized sensing devices. However, some information about materials and gases can be obtained exclusively through the use of advanced equipment only found on Earth [1]. Due to the overall complexity of the Mars Sample Return (MSR) mission, a very simple and reliable Earth Entry Vehicle (EEV) with passive reentry design is desired and is being developed [1,2]. The proposed design shown in Fig. 1 is without a parachute system and relies entirely on aerodynamic drag during reentry and an impact absorbing sphere to reduce the terminal velocity and peak impact acceleration down to levels where containment and survival of the enclosed material samples can be nearly guaranteed.

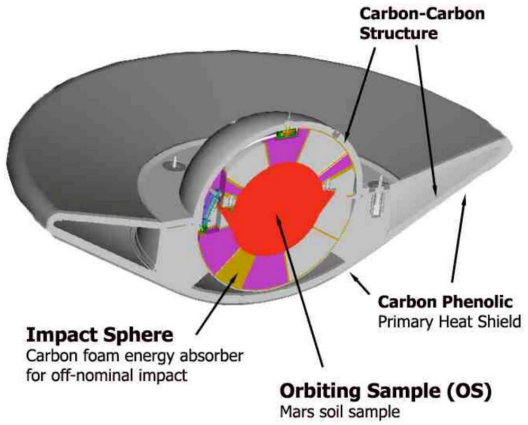

Fig. 1 MSR Earth Entry Vehicle [2]. *The relatively simple and lightweight structure has been designed for reliable passive Earth reentry and landing.*

A numerical analysis methodology has been created to aid in the design and evaluation of an EEV's structural components. This structural analysis methodology is being integrated into a larger system level analysis tool using a method proposed by Bayandor [3] and Samareh et al. [4]. The system level analysis tool [4] combines our structural dynamics module with four other modules such that all necessary aspects of the EEV design can rapidly be evaluated. The four other modules are an impact landing module [5], a thermal protection shield (TPS) module [6], an aerodynamics module [7], and a thermal soak module [8,9]. The analysis methodology allows parameters such as physical geometry, material properties, composite fiber orientation, loading, and payload mass to be quickly modified which allows an array of analyses to be conducted rapidly. Using the developed analysis methodology an engineer can then confirm quickly and with improved confidence that the chosen EEV design parameters are all within a feasible range and appropriate for the specific mission at hand. The ability of the analysis methodology to evaluate a broad range of mission scenarios and EEV designs is critical for optimizing EEV design and making the basic EEV architecture quickly modifiable for various future requirements.

2 The MSR Mission Plan

The MSR campaign was proposed by NASA and ESA and in 1998, the first official MSR project was created, initially in partnership with the Centre National d'Études Spatiales (CNES) [1]. In the past five years increased interest in the program has led to a flurry of research and design efforts. The numerical EEV analysis methodology devised and discussed in this paper is one aspect of the MSR mission efforts.

The MSR mission plan [1] is depicted in Fig. 2 with the path of the EEV highlighted with red arrows overlaying the figure. The MSR campaign begins with a mission to send equipment and rovers to Mars to collect Martian samples (not shown in the figure). Next an empty EEV with MSR Orbiter, is launched towards Mars. Upon reaching Mars the MSR orbiter begins to orbit Mars while awaiting samples to be delivered from the surface to it. Meanwhile on Mars, samples are collected by a rover and sealed within a spherical metallic canister called the Orbiting Sphere (OS). Subsequently, the MSR lander with Mars Ascent Vehicle (MAV) are sent to and landed on Mars where they rendezvous with the rover carrying the OS. The OS is then launched from the Martian surface aboard the MAV out to the MSR orbiter waiting in Mars orbit. The MSR mission has several planetary protection concerns and to protect Earth from uncontained Martian materials as well as to

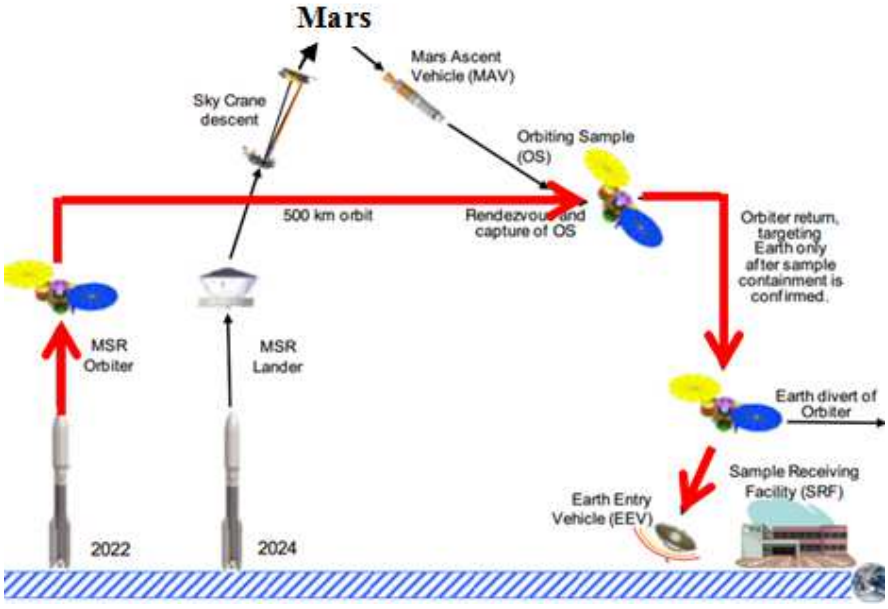

Fig. 2 The MSR Mission Plan [1]. *The mission cycle for the EEV is highlighted with red arrows.*

ensure the scientific integrity of the samples within, a special sample containment procedure must be followed in compliance with NASA NPR 8020.12 [10] and NASA NPR 8020.07 [11]. Once the sample laden OS reaches the orbiter the OS is sealed in the EEV and then the orbiter rockets back toward Earth on an orbital trajectory. Upon arrival to Earth orbit the EEV is released to enter into the Earth's atmosphere for return to the surface. During reentry, the EEV decelerates to an expected terminal velocity of approximately 40 m/s before impacting on the soft soil at the Utah Training and Testing Range [12]. For the mission to be successful, the EEV must be able to land with the samples contained at a high level of certainty [1].

3 Vehicle Design

The Multi-Mission Earth Entry Vehicle (MMEEV) is a stand-alone, modifiable Earth entry platform tailorable to different missions with different requirements. Previous sample return missions such as Genesis have had mishaps stemming from their design [13,14]. To reduce the risk of mission failure a passive reentry design is employed without complicated and potentially unreliable decelerating sub-systems such as parachutes or retrorockets.

As shown in Fig. 3, the vehicle has six basic components. First the OS contains the extraterrestrial samples. Next, encapsulating the OS, is the impact sphere (IS) which protects the OS and samples when the vehicle hits the Earth. Holding the IS and OS is the primary structure which withstands the structural and thermal loading during launch, reentry, and impact. The primary structure is comprised of four sub-components. The top structure is concaved in shape with a bulge in the middle that contours around the IS. The bottom structure has a blunt tipped cone shape and is the windward side of the vehicle during reentry. The rib structure is a circular ring that internally joins the top and bottom structures together and braced the vehicle. The structural foam component reinforces the EEV, thermally insulate the IS during reentry, and reduces the thermal soak into the IS that occurs primarily after Earth impact. Lastly, surrounding the exterior of the vehicle is a thermal protection system (TPS), which protects the vehicle against reentry heat.

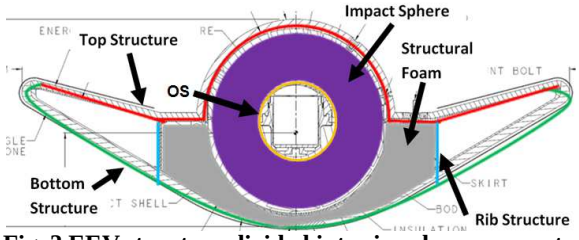

Fig. 3 EEV structure divided into six sub-components. *Non-structural TPS mass is also uniformly applied to the top and bottom structure.*

4 Modeling and Numerical Procedures

The devised analysis methodology is a technique in which the structural dynamic response of a parametric EEV configuration is rapidly evaluated. The first step is to build the structural dynamics model (SDM). An SDM is built in Patran using the Patran Command Language (PCL) [15]. PCL allows quick modification of input parameters for generating the finite element model. Thus new finite element models with different dimensions, materials, and section properties can be built for parametric investigations.

Since full EEV structural dynamics testing is still pending, experimental validation of the SDM is not currently possible. The parametric capabilities of the methodology are thus emphasized and the current MSR EEV design is preliminary. Note then that material properties, composite layups, dimensions, and other required values are estimates chosen only to demonstrate the capabilities of the methodology. Each sub-component depicted in Fig. 3 has a different element formulation and material model. A summary of the key finite element and mechanical properties is found in Table 1. The IS and OS have material properties consistent with those used in the Test 2 validation case in the IS impact report [5].

4.1 Parametric Model Assembly Features

Three key model building features facilitate reliable and automated parametric analysis. The features are: 1) the geometric variation and automated meshing capability, 2) the method of

Table 1. Selected Finite Element Model Properties

Component	Element Type	Material Model	E_{11} & E_{22}	Density	# of Plies	Thickness	Mass
Top Structure [16]	Cquad4 shell	Composite orthotropic	70 GPa	1600. kg/m^3	8	8 mm	4.57 kg
Bottom Structure [16]	Cquad4 shell	Composite orthotropic	70 GPa	1600. kg/m^3	8	16 mm	10.15 kg
Rib Structure [16]	Cquad4 shell	Composite orthotropic	70 GPa	1600. kg/m^3	8	12 mm	1.50 kg
Structural Foam [18]	Hex8 solid	Linear isotropic	180 MPa	110 kg/m^3	-	-	1.33 kg
Top TPS [17] (SLA-561V)	-	Non-structural mass	-	2.56 kg/m^2	-	-	1.80 kg
Bottom TPS [17] (Carbon Phenolic)	-	Non-structural mass	-	29.00 kg/m^2	-	-	22.99 kg
IS+OS	Shell/Solid	See Ref. 5	See Ref. 5	-	-	-	9.44 kg
						Total	**51.79 kg**

attaching the imported IS to the EEV, and 3) the way boundary conditions are assigned.

4.1.1 Geometric Variation and Automatic Meshing

Seven geometric parameters have been built into the code which allow SDMs to be built over nearly the entire EEV design space. Dimensions and angles can be varied, but new features cannot be created on top of an earlier model and existing features cannot be removed. The seven geometric parameters are shown in Fig. 4 and are listed with their base dimensions. A few extreme geometries were built and are presented in Fig. 5. Meshing of the model is quick and automated. Mesh density can be varied by a single parameter or through the combination of sub parameters.

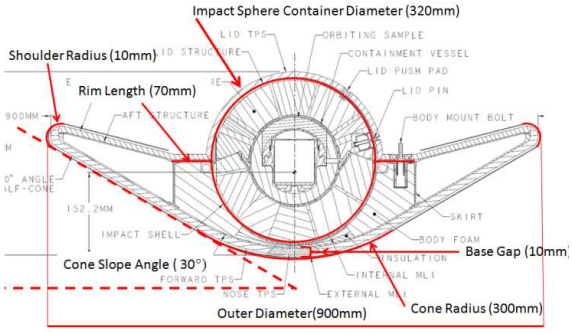

Fig. 4 The seven geometric parameters and their base configuration dimensions. *The parameters and dimensions are selected based on mission requirements.*

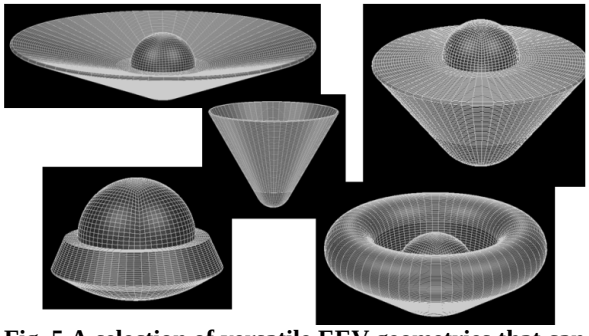

Fig. 5 A selection of versatile EEV geometries that can be constructed using the developed code.

4.1.2 Automatic Import and Attachment of the IS

The IS model is automatically imported and positioned at the center of the EEV. The IS model was built previously by the authors for the impact analysis module [5]. The IS model is attached to the EEV primary structure using a set of elastic 1D elements that connect two nodes together and are assigned stiffness and damping values. The elastic elements used to test the model have an axial stiffness similar to that of a short 3/8" steel bolt in order to simulate a stiff bolted connection between the IS and EEV.

The IS is connected to the EEV in two regions, the first is around the inner circumference of the rim and the second is in a small region at the base of the IS. The primary challenge in connecting the IS is to reliably automate the process for any mesh density and geometric variation. To address this issue a special PCL module was written and incorporated into the code that connects every node along the inner circumference of the EEV rim and every node inside a small region at the base of the EEV to a nearby node on the IS. The size of the base connection region can be adjusted parametrically as desired by the analyst. The module effectively generates a near rigid connection between the IS and the EEV primary structure and functions regardless of mesh density and geometric variation.

4.1.3 Assignment of Boundary Conditions and Thickening of Attachment Areas

The EEV will be launched into space aboard an Atlas or Delta launch vehicle. During launch the EEV is attached to a spacecraft that will orbit Mars until the EEV is loaded with the OS. The EEV is anchored at three locations equally spaced from each other on the rim area of the top structure. In order to comply with NASA spacecraft design and analysis standards [19,20] and to minimize the number of possible load paths through the structure, a minimally constrained set of grids were defined. The configuration removes indeterminacy from the analysis, makes verifications of the model via hand calculations simpler, potentially reduces analysis time, and also potentially vehicle weight [21]. During launch, the EEV is oriented with top and bottom structures facing perpendicular to the launch direction as shown in Fig. 6. In the figure the three attachment point indicated by red dots. The requirement for minimally constrained grids and the orientation of the EEV during launch demands a different set of constraints for each attachment area. The constrained degrees of freedom at each location are indicated by green arrows next to the red dots in Fig 6. The attachment point located at the highest point with respect to the launch orientation has X, Y, and Z translational degrees of freedom constrained. The lower left attachment points has X and Y degrees of freedom constrained. The lower right attachment point has only the Y degree of freedom constrained. This configuration is confirmed to generate rigid body motion in all directions using a standard 1 G acceleration technique [22].

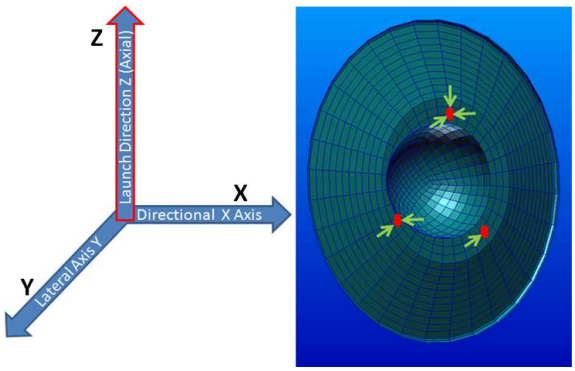

Fig. 6 EEV launch orientation and minimally constrained BCs at the three attachment points. *The green arrows show the directions in which each red dot area is constrained.*

A specialized PCL module was developed to assign constraints reliably to any possible geometry and mesh variation. The module works by finding nodes in three parametrically defined regions on the upper rim surface. Each region is defined in cylindrical coordinates and has the shape of an arc with an inner and outer radius. The thickness of each arch is limited to the middle third of the rim surface and the angular position and width of each arc is defined by the relationship $120n \pm 10°$, where n = 0, 1, 2. All the surface nodes found in the regions are assigned the specified boundary condition and every element adjacent to a constrained node is thickened 50% more than the normal thickness of the top surface. The module has been fine-tuned so that only one radial set of nodes are selected and constrained. Also the mesh settings have been assigned so that no less than two nodes will be assigned at each attachment area. These code refinements were implemented to ensure the same type of constraints are present in the model regardless of mesh density. This is an important feature for dynamic vibration analysis.

4 Analysis Coding and Implementation

The analysis methodology that was created evaluates the structural response of an EEV during the launch portion of a mission caused by different physical phenomenon. The required analyses have been subdivided into three groups: 1) quasi-static launch loading, 2) structure-borne vibration frequency response, and 3) random acoustic.

4.1 Quasi-Static Launch Loading Analysis

The quasi-static analysis evaluates the structural response of the EEV due to launch accelerations. The attachment constraints described in 4.1.3 are applied. An inertial loading envelope for one potential launch vehicle was provided by NASA and is presented in Fig. 7. The vertical axis is the axial (launch direction) axis and the horizontal axis is the lateral (orthogonal to launch direction) axis. A list of potential ‘worst-case’ load cases was

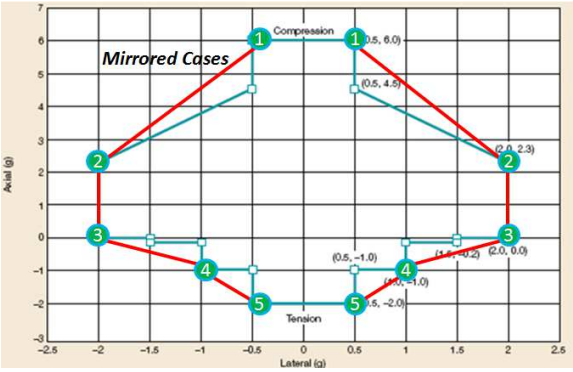

Fig. 7 The inertial load envelope for one possible launch vehicle with overlaid load case information. *During launch the inertial loads are primarily in the launch direction, however significant forces are also found the transverse directions.*

developed by selecting points along the perimeter of the envelope. The lateral direction inertial vectors can have a positive or negative value so the five points listed in the figure are also mirrored to have an additional five cases. Additionally because the EEV is not axisymmetrically attached on the rocket during launch, both directions orthogonal to the launch direction need to be considered independently. Thus, the number of quasi-static inertial load cases doubles from 10 to 20. All 20 load cases are evaluated and incorporated into the PCL code. The load case information can quickly be changed to account for different launch vehicles. For each sub-case, the von Mises stress field data is output for all elements. Maxiumum principle stresses for each ply can also be output for detailed analysis of the laminated composites.

4.2 Structure-Borne Vibration Frequency Response Analysis

The frequency response analysis evaluates the affect of structural vibrations coming from the launch vehicle. The modal response of the vehicle and peak resonant acceleration are recovered. A 1 m/s^2 unit acceleration sinusoidal base excitation is applied at each attachment point. The modal response of the vehicle is recovered from 20 Hz to 400 Hz. If the analyst desires a broader frequency range to be evaluated, it can quickly be changed in the PCL code. A lumped mass formulation is used. For demonstration purposes the acceleration frequency response of five different nodes is

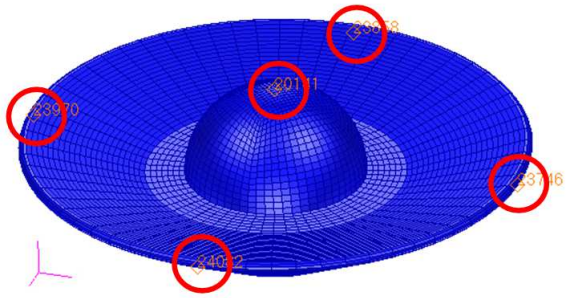

Fig. 8 Node locations for acceleration frequency response output. *Five nodal locations were selected to attain a preliminary vehicle frequency response.*

output. The node locations, shown in Fig. 8, have been parameterized so that they remain in the same location regardless of mesh density or geometric variation. Later, the settings can quickly be modified so that stress data is output for specific elements or the whole model.

4.3 Random Acoustic Analysis

The random acoustic analysis evaluates the structural response of the EEV from broad spectrum high intensity noise induced by the rocket boosters during launch. In fragile, light weight space structures, high intensity noise can cause structural damage and hence random acoustic analysis must be conducted. For this analysis, NASA provided a broad spectrum acoustic pressure plot for one possible launch vehicle. To run a random acoustic analysis first a pressure frequency response analysis is conducted with a 1 Pa pressure applied uniformly to the external surface of the EEV. Then output data from the pressure frequency response analysis is input into a separate random analysis module in Patran. The multi-step process has been fully automated in the developed PCL code.

NASA often conducts acoustic analyses up to 2000 Hz according to test specifications [23], so the NASA acoustic data was converted from dB into pressure PSD from 20 Hz to 2000 Hz and is presented in Fig. 9. The data in the figure has been entered into the PCL code and can be modified if necessary to accommodate analyses for different launch vehicles. The standard attachment constraints as defined in section 4.1.3 are also used for this analysis. Von Mises root-mean-squared (RMS) von-Mises stress data for all elements is output by the solver.

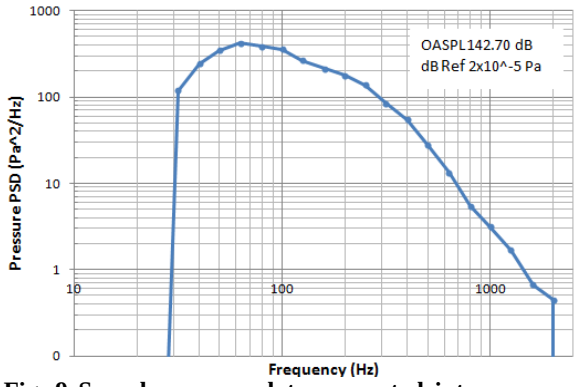

Fig. 9 Sound pressure data converted into pressure PSD format from 20 to 2000 Hz. *Data was data was bounded from 20 to 2000Hz according to NASA acoustic test specifications [23].*

5 Model Verifications and Checks

It is recognized that model verifications and checks are no comparison to validations against experimental data. In the future as experimental data becomes available a full validation of the developed methodology should be conducted. In the absence of such validations the SDMs and the PCL code were continuously checked and verified throughout the development process.

Standard NASA mandated model checks were completed on SDMs built using the developed methodology [22]. These checks include prescribed unit displacement checks, free-free dynamics checks, unit gravitational loading checks, and extensive element shape and formulation checks. The automatic meshing portion of the developed code has been extensively tuned to produce elements with acceptable aspect ratios and curvatures for all mesh factors. All elements in the primary EEV structure pass standard Nastran geometry checks. Coincident element checks were completed and duplicate nodes are automatically removed from the model during the build process. Element normals were also checked and normals are automatically reversed where necessary. Mass checks were also completed and the model mass calculations have been verified independently with hand calculations.

In addition to the model verification checks, the analysis methods were tested on simpler models where results could independently and more simply be verified. For the quasi-static case, a simple single element study was completed to show that correct reaction forces and stresses could be recovered from the inertial loading. For the frequency response analysis a beam model with a known exact solution was modeled and the Nastran results matched a hand solution as well as results from other FE codes. For the random acoustic analysis an aluminum cantilevered beam was independently modeled using the same NASA practices [23]. The results of that model perfectly matched the results from the NASA benchmark provided in Ref. 23.

6 Simulation Results from Parametric Variation

To demonstrate the parametric features of the analysis methodology, mesh density and cone angle parameters were varied. For mesh density, a single parameter called "mesh factor" (MF) was used to scale the mesh generation. Mesh factors 1 (low density), 2 (medium density), and 3 (high density) were evaluated. Cone angles of, 20°, 30°, and 40° were evaluated. The base configuration has the geometry shown in Fig. 4, a MF of 2, and a cone angle of 30°.

6.1 Quasi-Static Launch Loading Results

As described previously, 20 load cases are run by executing the PCL code. Thus, by evaluating five different SDMs together for mesh density and cone angle, a total of 100 different results were generated. Table 2 summarizes the quasi-static inertial analysis finding for both mesh and cone angle. Trends from the mesh study are initially perplexing because no convergence is observed. The lack of convergence is caused by the combined effect of the method in which the model is meshed, the automated method of assigning attachment point area thicknesses, and limited number of possible nodal constraint locations which lead to variations in the effective

Table 2. Key Inertial Loading Results

Mesh Factor	1	2	3
Peak Stress, MPa	3.38	3.11	3.64
Cone Angle	**20°**	**30°**	**40°**
Peak Stress, MPa	3.37	3.11	3.64

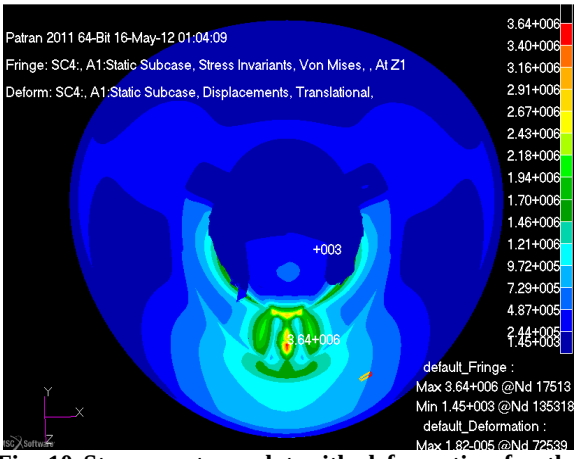

Fig. 10 Stress contour plot with deformation for the high density mesh sub case with the largest max stress configuration model. *For this load case motion is only restrained by one of the attachment points. Most of the stress is thus concentrated around this attachment point.*

attachment area size. Thus when an analyst attempts to converge the results using mesh density, elements away from the attachment points should be used. After the results were generated, the module for meshing the attachment surface and assigning BCs was improved to make it consistent regardless of mesh factor. This should yield more predictable results in future use. Figure 10 shows the stress contour with deformation for the high density mesh case with the highest max stress. Additionally for the cone angle study peak stress was observed to increase both by decreasing and increasing the angle away from the baseline. This is caused by the increased offset of the vehicle CG away from the attachment points in the 20° case and the increased vehicle weight (larger bottom structure surface area and thus heavier TPS) in the 40° case.

6.2 Frequency Response Results

For each parametric variation of the model the model was excited in each orthogonal direction (X, Y, Z). The acceleration response in each

Table 3. Key Frequency Response Results

Mesh Factor	1	2	3
First Mode, Hz	390	355	355
Cone Angle	**20°**	**30°**	**40°**
First Mode, Hz	333	355	365

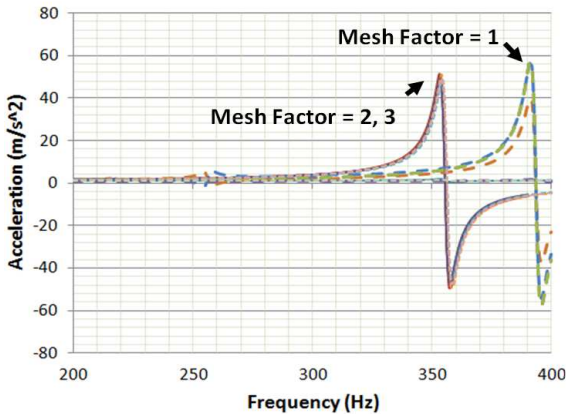

Fig. 11 Y direction frequency response plot for different mesh densities. *A change in the first resonant frequency was found between MF 1 and 2, but between MF 2 and 3 the differences are small.*

orthogonal direction was recovered for the nodal locations mentioned in section 4.2. The largest peak response was observed in the Y direction induced by a Y direction excitation. This is an excitation along the axisymmetric axis of the vehicle. The key results for the mesh density frequency response analysis are found in Fig. 11 which shows the Y direction frequency response plot due to a Y direction base excitation. Table 3 summarizes the findings. The unusually sharp drop in the first mode frequency might be considered counter intuitive based on finite element convergence theory for a lumped mass model. However, the reason for the unexpected reverse type convergence lies again in the way that the attachment nodes were assigned and the way that the attachment areas were reinforced to reduce localized stress concentrations. For the low mesh density configuration, the limitation in

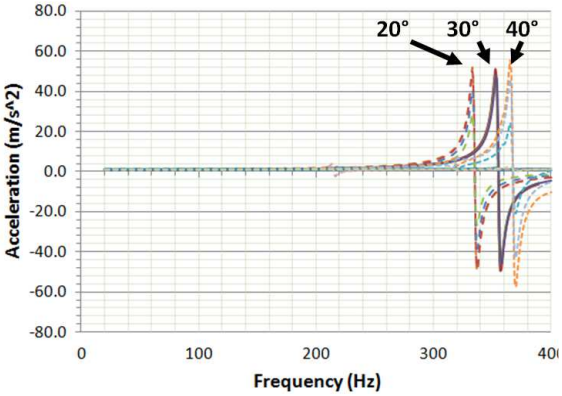

Fig. 12 Y direction frequency response plot for different cone angles. *Increasing the cone angle from 20 to 40 degrees successively increases the first resonant frequency*.

possible nodal attachment points results in a larger BC footprint and a larger stiffened section thereby giving the vehicle a stiffer response. Because the frequency response curves for MF 2 and MF 3 look almost identical, the model is considered to have reached an acceptable level of convergence for this analysis.

The key results for the cone angle frequency response analysis are found in Fig. 12 which presents the frequency response plot for the different cone angles. It can be seen from the table and figure that as cone angle is increased from 20° to 40°, the first natural frequency is increased but the magnitude of the resonance remains about the same for each case.

6.3 Random Acoustic Results

The effects of mesh density on the random acoustic results were investigated. Key results for both the mesh density and cone angle analysis are found in Table 4. The change between the MF 1 and 2 is 38% whereas the change between 2 and 3 is only 6%. Thus for preliminary analysis sufficient accuracy is achieved at MF 2. If higher accuracy is required, the MF can be increased to 4 or higher. Fig. 13 shows the 20° and 40° cone angle RMS von Mises stress fringe plots. Notice the rings of high and low stress on the surface of the structure. These rings are representative of the resonance mode shape of the EEV when excited. In addition to peak stress values the overall stress gradients are also of interest. In the 20° model, the high stress areas are spread out quite evenly across the surface of the EEV. However, for the 40° model, the stress becomes much more localized near the attachment points. Using this information the structural thickness of the composite material can be chosen to lower the overall mass.

Table 4. Key Random Acoustic Results

Mesh Factor	1	2	3
Peak Stress, MPa	0.50	0.76	0.81
Cone Angle	**20°**	**30°**	**40°**
Peak Stress, MPa	0.80	0.76	0.86

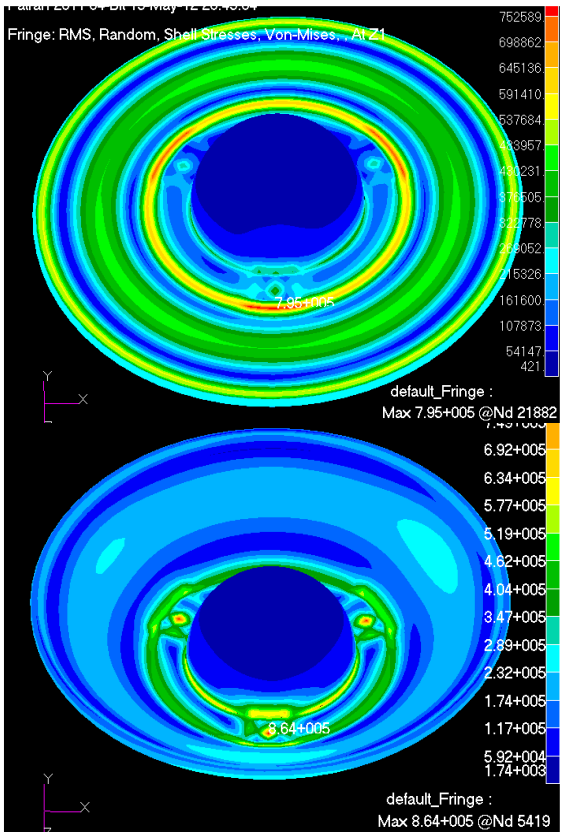

Fig. 13 Low angle cone angle vs. high angle cone angle stress contour plots. *Notice the dramatically different stress distribution as a result of changing the cone angle from 20° to 40°.*

7 Conclusion and Recommendations

The structural dynamics analysis methodology discussed has been created to be highly parametric and provide an advanced capability to aid and accelerate the development of future EEVs for NASA sample return missions. The most notable of these missions is MSR planned for launch in the mid-2020s. In this phase of EEV development, attention was paid to the evaluation of the structural response of the EEV to inertial launch loading, structure-borne vibrational loading, and random acoustic loading. Using the developed methodology, it was shown that the structural response of numerous possible EEV designs can be determined rapidly and with minimal effort by a mission analyst. The mesh study determined that stress concentrations near the attachment points to the carrier spacecraft caused issues with maximum stress based convergence. As a result stresses near the attachment points should be viewed with speculation. Data from the frequency response and random acoustic analyses indicated

convergence was achieved at a mesh factor of 2-3. For the cone angle study, the most prominent observation was that increasing the cone angle resulted in a frequency shift of the EEV's first mode. Due to the lack of experimental testing, extensive verifications and sub-validations of the methodology were conducted. In future, a detailed validation effort will be attempted as experimental data becomes available. In summary, the reported work conducted under the MSR Program marks a direct contribution to future space and planetary exploration missions.

8 Acknowledgements

This project was funded by the NASA In-Space Propulsion Technology (ISPT) program. Dr. Jamshid Samareh and Dr. Sasan Armand of NASA Langley, Mr. Bo Walkley of the National Institute of Aerospace, and Mr. Aaron Horning of Analytical Mechanics Associates, Inc. were pivotal in the success of this project.

9 References

[1] R. Mattingly, L. May, Mars Sample Return as a Campaign, in: IEEE Aerosp. Conf., IEEE, Big Sky, MT, 2011.

[2] R.W. Maddock, Sample Return Challenges Multi-Mission Earth Entry Vehicle Design Trade Space and Concept Development Strategy, in: 6th Int. Planet. Probe Work., IPPW, Atlanta, GA, 2008.

[3] J. Bayandor, D.J. Elder, M.Q. Nguyen, Unification Options for the Impact and Damage Analysis Tool (IDAT), Melbourne, Australia, 2003.

[4] J.A. Samareh, R.W. Maddock, R.G. Winski, An Integrated Tool for System Analysis of Sample Return Vehicles, in: Big Sky, MT IEEE Aerosp. Conf., IEEE 2012 Aerospace Conference, Big Sky, MT, 2012.

[5] S.V. Perino, J. Bayandor, A. Siddens, A Comprehensive Structural Dynamic Analysis Approach for Multi Mission Earth Entry Vehicle (MMEEV) Development, NASA STI. 2013.

[6] J.E. Johnson, M.J. Lewis, R.P. Starkey, Multiobjective Optimization of Earth-Entry Vehicle Heat Shields, J. Spacecr. Rockets. 49 2012.

[7] R.A. Mitcheltree, C.M. Fremaux, L.A. Yates, Subsonic Static and Dynamic Aerodynamics of Blunt Entry Vehicles, in: 37th AIAA Aerosp. Sci. Meet. Exhib., AIAA, Reno, NV, 1999.

[8] R.M. Amundsen, J.A. Dec, R.A. Mitcheltree, R.A. Lindell, R. Dillman, Preliminary Thermal Analysis of a Mars Sample Return Earth Entry Vehicle, in: 34th AIAA Thermophys. Conf., AIAA, Denver, CO, 2000.

[9] P. Agrawal, S.A. Sepka, J.F. Aliaga, E. Venkatapathy, J.A. Samareh, Thermal Soak Analysis of Earth Entry Vehicles, in: 43rd AIAA Thermophys. Conf., AIAA, New Orleans, LA, 2012.

[10] S.M. Directorate, NASA NPR 8020.12D Planetary Protection Provisions for Robotic Extraterrestrial Missions, Washington, DC, 2011.

[11] S.M. Directorate, NASA NPR 8020.7G Biological Contamination Control for Outbound and Inbound Planetary Spacecraft, Washington, DC, 1999.

[12] N.C. Bauer, B.P. Smith, C.L. Tanner, D.A. Spencer, Multi-Mission Earth Entry Vehicle Impact Analysis, Atlanta, GA, 2009.

[13] NASA, Genesis Mishap Investigation Board Report Vol 1., Washington, DC, 2005.

[14] W.H. Willcockson, Stardust Sample Return Capsule Design Experience, AIAA J. Spacecr. Rocket. 36 1999.

[15] MD Nastran Quick Reference Guide MD Nastran 2011 & MSC Nastran 2011 Quick Reference Guide, 2012th ed., MSC Corp., Santa Ana, CA, 2011.

[16] W. Hyer, S.R. White, Stress Analysis of Fiber-Reinforced Composite Materials, DEStech Publications Inc., 2009.

[17] B. Laub, Thermal Protection Concepts and Issues for Aerocapture at Titan, in: 39th AIAA Jt. Propuls. Conf. Exhib., AIAA/ASME/SAE/ASEE Joint Propulsion Conference and Exhibit, Huntsville, AL, 2003.

[18] Rohacell WF Foam Properties, (2013) 7573.

[19] NASA-STD-7009 Standard for Models and Simulations, Washington, DC, 2008.

[20] NASA-STD-5002: Load Analysis of Spacecraft and Payloads, Washington, DC, 1996.

[21] W. Harkins, NASA Public Lessons Learned: Structural Stress Analysis, Greenbelt, MD, 1999.

[22] FEMCI Book, Finite Element Model Validity Checks, NASA, 2006.

[23] FEMCI Book: NASTRAN Random Vibration, NASA, 2006.

Copyright Statement